ACS OMEGA

http://pubs.acs.org/journal/acsodf

Article

Enhanced Bactericidal Action of rGO−ZnO Hybrids Prepared by the One-Pot Co-precipitation Approach

Osama Usman, Muhammad Ikram,* Namra Abid, Mohsin Saeed, Aneeqa Bashir, Walid Nabgan,* Nosheen Mushahid, and Mujtaba Ikram*

Cite This: *ACS Omega* 2022, 7, 26715−26722

Read Online

ACCESS | Metrics & More | Article Recommendations

ABSTRACT: Metal-based antimicrobials have the potential to profile sustainable solutions to infection care and health. In this study, we report the synthesis of rGO−ZnO hybrid nanostructures by a simple co-precipitation approach with various mass ratios of GO, and their antimicrobial potential was assessed. The structural analysis confirms the presence of a hexagonal wurtzite structure with peak shifting in hybrid nanostructures and increases in crystallite size (11−24 nm). Raman spectra revealed GO doping in the D band (1350 cm^{-1}) and G band (1590 cm^{-1}). Field emission scanning electron microscopy (FESEM) and transmission electron microscopy (TEM) were performed to investigate the surface morphologies of the synthesized sediments, which showed a change in the morphology of ZnO from non-uniform spherical nanoparticles to a rod-like morphology of the prepared hybrid nanostructures. RAMAN spectra revealed that the retained functional groups on rGO planes were significant in anchoring ZnO to rGO. At lowest and maximum doses of ZnO, substantial bactericidal zones ($p < 0.05$) for *S. aureus* (1.55 and 1.95 mm) and *E. coli* (1.25 and 1.70 mm) were achieved accordingly. Additionally, the inhibition regions were 2.45−3.85 mm and 3.75−6.85 mm for *S. aureus* whereas (2.05−3.25 mm) and (2.95−3.90 mm) for *E. coli* at the lowest and maximum concentrations.

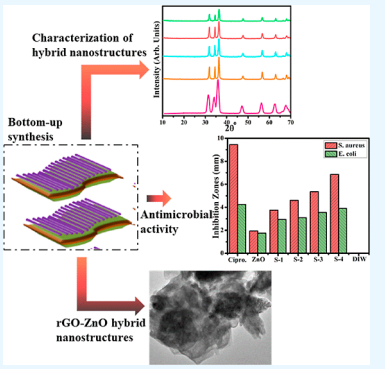

1. INTRODUCTION

Infectious diseases are emerging, and antibiotic resistance is spreading across a variety of disease causing bacteria, posing a severe threat to global public health. Furthermore, the bioactivity of the produced antibiotics is of equal role in maintaining its safe clinical application. Along with antimicrobial therapy, the morbidity and mortality rates associated with bacterial infections remain high, owing in part to the bacterial ability to acquire resistance to practically all antibiotics. To discover and promote the next generation of antibacterial medications or agents, new strategies are required. Nanomedicine has recently gained popularity as a potential antibacterial active material.[1−3] In the current materials science, nanotechnology is a popular research area. Nanoscale materials (1−100 nm) can be used for a variety of novel applications, including innovative fabric compounds, food processing, and agricultural production, as well as advanced pharmaceutical treatments. The characteristics and functions of living and anthropogenic systems are defined at this level.[4]

Since ancient times, humans have relied on the antibacterial properties of many metals such as Ag, Al, Cd, Cu, Ni, Zn, and so forth.[5,6] The ability of metal ions to inhibit enzymes, facilitate the generation of reactive oxygen species causing cell membrane damage, and prevent the uptake of vital microelements by microbes is the foundation of metal antimicrobial activity. Furthermore, several metals can exert direct genotoxic activity.[7] Metal oxide nanoparticles, such as silver, gold, copper, titanium oxide, and zinc oxide (ZnO), have been reported to be the most antibacterial inorganic materials.[8,9] ZnO is the most potential inorganic material among metal oxides, having a diverse variety of uses: (1) as a filler and rubber compound activators in the rubber industry, (2) as a cream, powders, and dental pastes in the pharmaceutical and cosmetics industries, (3) as UV radiation absorbers in the textile sector, (4) as photoelectronic, field emitters, sensors, UV lasers, and solar cells in the electrotechnology and electronics sector, and (5) as a photocatalyst in photocatalysis. Other important uses for zinc oxide include the fabrication of zinc silicates, criminal analysis/fingerprint augmentation, and packaging. In comparison to TiO_2, ZnO has a 3.3 eV comparable band gap energy and a modest production cost.[10,11]

Apart from the antibacterial properties of ZnO nanostructures, many researchers have tried to improve them by manufacturing composites with metal oxides or doping other

Received: May 16, 2022
Accepted: July 13, 2022
Published: July 25, 2022

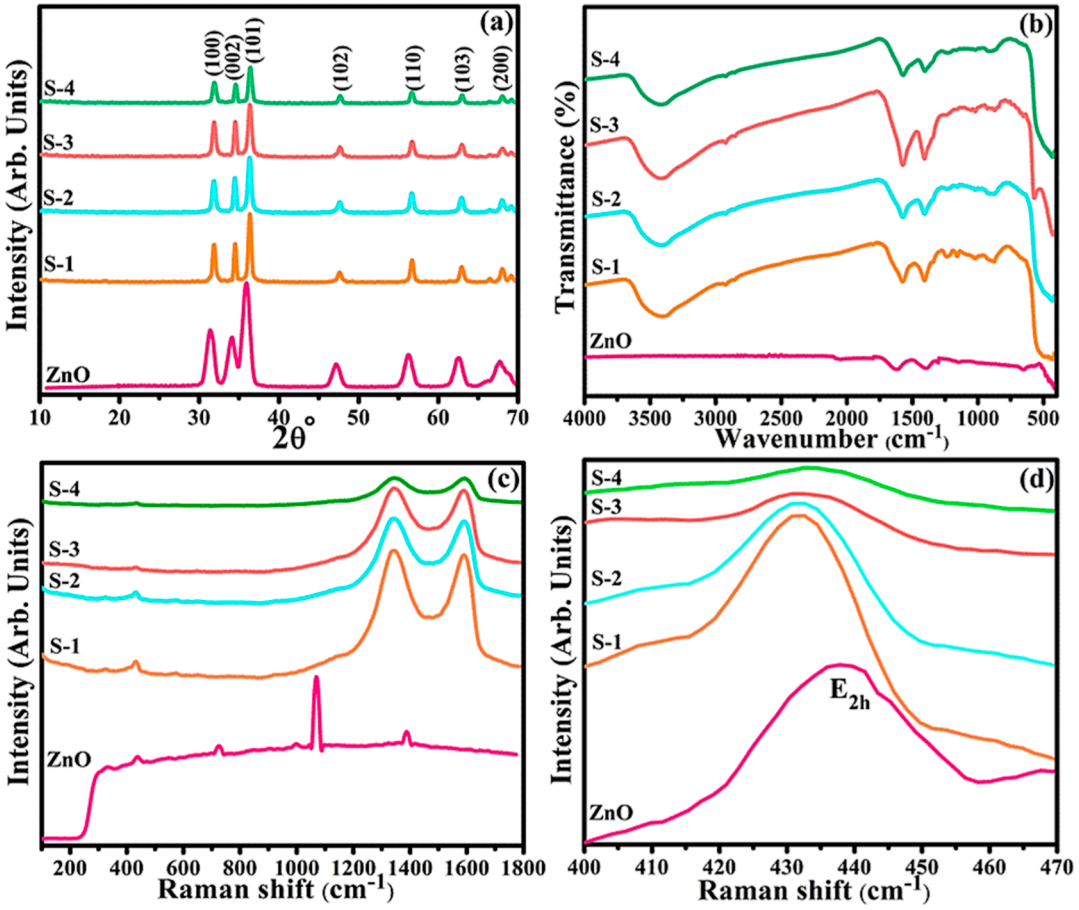

Figure 1. (a) XRD, (b) FTIR, (c) Raman spectra, and (d) zoom-in of Raman spectra of ZnO and rGO−ZnO hybrids.

ions as impurities.[12−15] ZnO limitations such as photo deterioration under UV irradiation, electron−hole recombination, lack of visible light absorption, and aggregation are most likely to be responsible for this improvement.[16] According to reports, graphene, a thin sheet of carbon atoms, has caught the interest of scientists due to its unusual mechanical, electrical, and optical capabilities. Carbon nanotubes, fullerenes, and graphite are all made up of graphene, which may be rolled, curled, and stacked to make carbon nanotubes, fullerenes, and graphite.[17−19] Over the last few decades, graphene oxide (GO), reduced graphene oxide (rGO), and graphene-based material electrodes have been shown to be a successful replacement to traditional mercury electrodes for heavy metal trace detection. The reduction of graphene oxide produces the majority of the graphene or reduced graphene oxide layer utilized in electrochemistry, which has functional groups such as hydroxyl and carbonyl, which are advantageous for absorbing heavy metal ions.[20] rGO in a composite structure with different semiconductor materials is used in many practical applications.[21−27] Low-dimensional semiconducting nanostructures combined with 2D carbon-based materials form hybrid nanostructures with interesting optoelectronic features. The manufacturing of supercapacitors, photocatalysis, photodetectors, and solar cells could all benefit from the hybridization of 2D carbon-based materials with ZnO.[28−33] In this work, we used a one-pot co-precipitation method to synthesize rGO−ZnO hybrid nanostructures and investigated their enhanced antimicrobial activity.

2. RESULTS AND DISCUSSION

XRD was used to characterize samples for structural and phase composition investigation, Figure 1a. ZnO peaks were observed at $2\theta^\circ$ = 31.7, 34.4, 36.2, 47.5, 56.5, 62.8, and 68.0° corresponding to the crystallographic planes (100), (002), (101), (102), (110), (103), and (112), respectively. These planes are in good agreement with (JCPDS no. 36-1451), indicating that a hexagonal wurtzite structure has formed.[34] Furthermore, no GO- or rGO-related peaks have been found. This is because during the fabrication of rGO−ZnO hybrids, GO was decreased and exfoliated.[35] Moreover, upon addition of rGO, the peaks shifted to higher $2\theta^\circ$, and with an increasing concentration of rGO in ZnO, the intensity of peak (101) decreases gradually. The characteristic diffraction peak of rGO is not seen in the XRD patterns of hybrids, which is owing to the lower content during hybrid structure formation, and the ZnO nanoparticles prevent carbon nanosheets from restacking.[36] Using the Debye−Scherrer formula, the crystallite size of the pure sample was found to be 11 nm and was found to increase from 19 to 24 nm, for increasing concentration of GO. This change is attributed to the functional groups of GO, and chemical reduction of GO to rGO serves as the nucleation site for the growth of ZnO nanorods.[37]

FTIR spectroscopy was used to further investigate the functional groups of the produced materials, Figure 1b. The Zn−O stretching mode corresponds to the peak between 600 and 400 cm^{-1}. The vibrational frequency owing to the ZnO lattice is shown by the peak at 879 cm^{-1}.[38−40] The intense

https://doi.org/10.1021/acsomega.2c03049
ACS Omega 2022, 7, 26715−26722

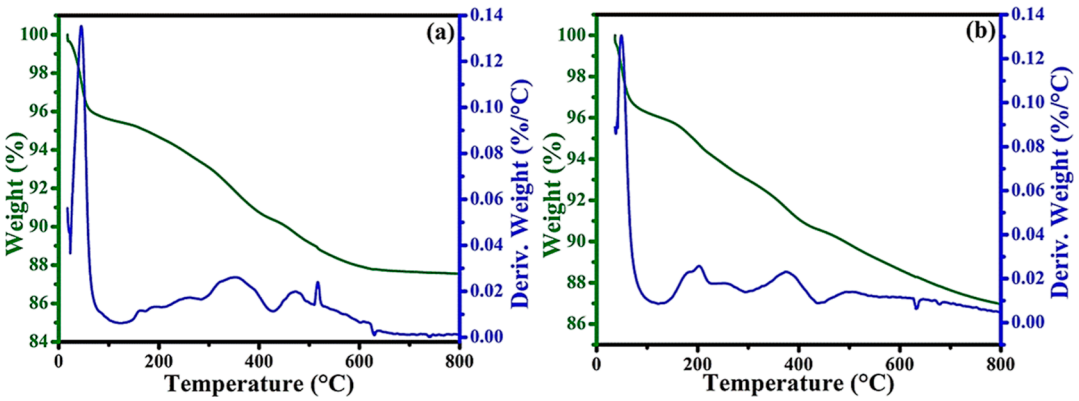

Figure 2. DSC/TGA curves of (a) S-1 and (b) S-2 in nitrogen.

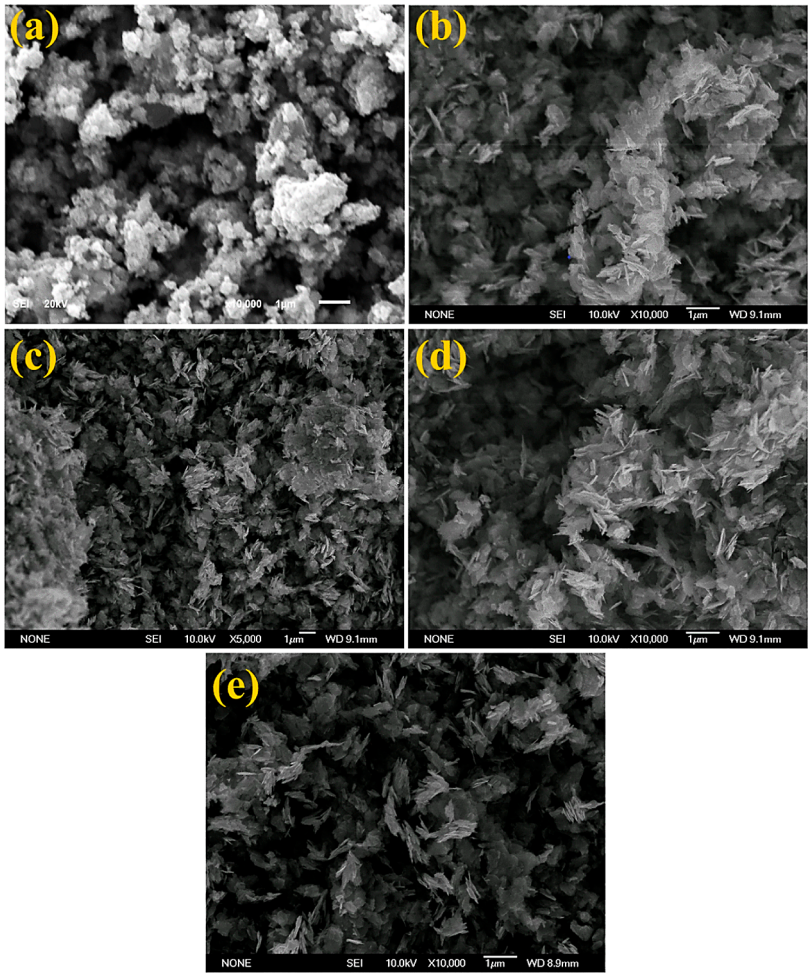

Figure 3. SEM of ZnO (a) and rGO−ZnO hybrids (S-1, S-2, S-3, and S-4) (b−e), respectively.

band at 3400 cm^{-1} is due to −OH stretching;[41] the O−H stretching vibrations of the carboxylic group are reflected in the peak at 1395 cm^{-1}.[42] The C═C vibrations produced by the aromatic ring mode account for the peak at 1570 cm^{-1}.[43]

Raman spectroscopy was used to examine the surface structure and disorder of the synthesized samples, as shown in Figure 1c. The peaks at 437 cm^{-1}, E_2^{high} (E_{2h}) in zoom-in Figure 1d, and 725 cm^{-1} (LA + TO) are assigned to multi-phonon scattering processes, and a prominent peak at 1069 cm^{-1} is in the E_2H characteristic mode of wurtzite structure of ZnO.[44−46] A minor peak at 1386 cm^{-1} occurred due to the high fluorescent background.[47] Peaks at 1350 and 1590 cm^{-1} correspond to the D and G bands, respectively. The existence of sp^2 carbon is represented by the G peak, whereas the presence of disorder in the graphene structure is shown by the D peak. The D and G peaks indicate that the structure of rGO is conserved in hybrids.[48]

The active material content of the rGO−ZnO (S-1 and S-2) hybrids was determined by employing thermogravimetric analysis (TGA) and differential scanning calorimetry (DSC) in a nitrogen atmosphere in a temperature range of 0−800 °C (Figure 2). The removal of the absorbed water molecules/

https://doi.org/10.1021/acsomega.2c03049
ACS Omega 2022, 7, 26715−26722

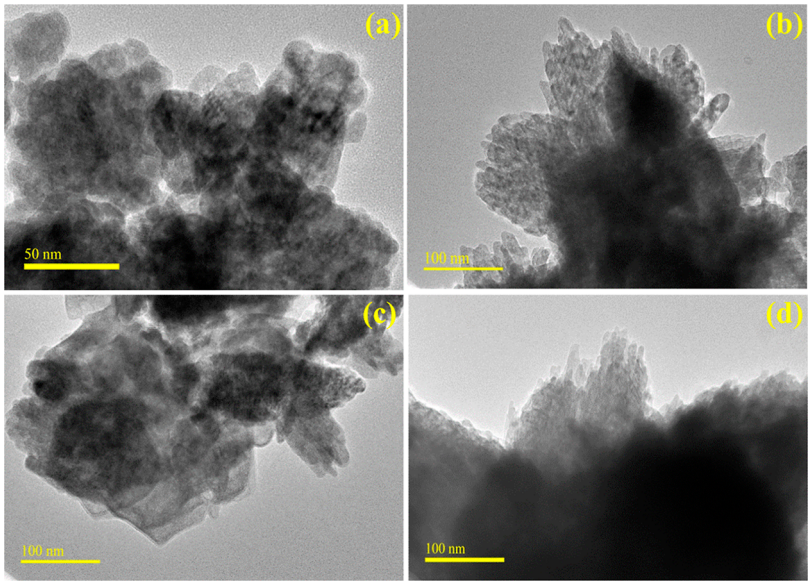

Figure 4. TEM of (a) ZnO and (b−d) S-2, S-3, and S-4, respectively.

Table 1. Microbicidal Action of rGO−ZnO Hybrid Nanostructures

	[a]inhibition zone (mm)		[b]inhibition zone (mm)	
sample	500 μg/50 μL	1000 μg/50 μL	500 μg/50 μL	1000 μg/50 μL
ZnO	1.55	1.95	1.25	1.70
S-1	2.45	3.75	2.05	2.95
S-2	2.90	4.60	2.75	3.10
S-3	3.35	5.35	3.25	3.55
S-4	3.85	6.85	3.65	3.90
ciprofloxacin	9.45	9.45	4.25	4.25
DIW	0	0	0	0

[a]Inhibition regions of doped nanostructures for *S. aureus*. [b]Hybrid nanostructures areas of inhibition (mm) against *E. coli*.

bound OH groups from the material surface causes the initial weight loss between room temperature and 120 °C. The removal of carbon molecules from the graphene structure backbone could explain the second weight reduction from 250 to 450 °C.[49] The loss up to 800 °C can be attributed to the removal of the remaining carbonyl groups.[50,51]

FESEM was performed to analyze the microstructure and morphology of the prepared samples, and the resulting micrographs are shown in Figure 3. Figure 3a depicts the SEM image of ZnO nanostructures, revealing a non-uniform spherical particle-like morphology, and particles are agglomerated and no complete separation has occurred. The high surface energy of nanoparticles could be the cause of particle aggregation.[52] Figure 3b−e shows rGO−ZnO hybrids with different concentrations of GO (10−40 mg), respectively. In Figure 3b, ZnO particles seem to be embedded on rGO sheets, and few rod-like morphologies can be observed. With the increasing concentration of GO, Figure 3c,d, the rod-like structure seems to be improved, but at the maximum concentration, Figure 3e, the agglomeration of the structures occurs and the rods are aggregated. As a result, an increase in GO concentration has a synergistic impact that regulates dimensional ZnO production by regulating the dimensional ZnO nanostructures from nanoparticles to nanorods.[53]

TEM micrographs of ZnO and rGO−ZnO hybrids are shown in Figure 4a−d, respectively. Corresponding to the SEM images, pristine ZnO has aggregated particles forming a cluster-like structure (Figure 4a). Addition of rGO into ZnO showed that a needle-like morphology with increased agglomeration of ZnO clusters was observed (Figure 4b). Aggregation seems to increase with the increasing concentration of GO into the reference sample (Figure 4c). The maximum amount of GO in ZnO showed high aggregations with elongated needle-/rod-like structures, Figure 4d.

The in vitro bactericidal behavior of pure and doped materials toward pathogens was determined using the well diffusion technique as presented in Table 1. All samples were positive for the antibacterial action toward bacterial pathogens. The findings indicated an additive impact between the synthesized samples and inhibitory zones. At lowest and maximum doses of ZnO, substantial bactericidal zones ($p < 0.05$) for *S. aureus* (1.55 and 1.95 mm) and *E. coli* (1.25 and 1.70 mm) were achieved, accordingly. Additionally, the inhibition regions were 2.45−3.85 mm and 3.75−6.85 mm for *S. aureus* whereas 2.05−3.25 mm and 2.95−3.90 mm for *E. coli* at lowest and maximum concentrations, correspondingly. These findings were contrasted to those acquired with ciprofloxacin as 9.45 and 4.25 mm for *S. aureus* and *E. coli* in comparison to DI water 0 mm, respectively. As compared to Gram-positive bacteria, pristine and doped specimen showed remarkable antibacterial activity against Gram-negative bacteria, as Gram-positive bacteria lack an outer lipid membrane and have a thick peptidoglycan layer instead. Additionally, it is possible that RGO aided absorption of Zn^{2+} into microbial

https://doi.org/10.1021/acsomega.2c03049
ACS Omega 2022, 7, 26715−26722

Table 2. Antimicrobial Activity of rGO−ZnO Hybrid Nanostructure Literature Comparison with the Current Work

materials	synthesis route	bacterial strains	testing method	concentration	remarks	reference
rGO−ZnO	green	*Cocci* and *E. coli*	well diffusion	10, 20 and 30 μg/mL	> for G +ve	65
rGO−ZnO	one-pot	*E. coli*	disc diffusion	50 mg/mL	effective	66
rGO−ZnO	green	*S. aureus* and *E. coli*	broth dilution	2.5 mg	> for G −ve	67
rGO−ZnO	hydrothermal	*K. pneumonia*, *B. thuringiensis*, *B. cereus*, and *P. aeruginosa*	well diffusion	20, 30 and 50 μL	> for G +ve	68
rGO−ZnO	co-precipitation	*S. aureus* and *E. coli*	well diffusion	0.5 and 1.0 mg/50 μL	> for G +ve	present study

cellular membrane and increased permeation of metal ion (Zn^{2+}) while also dislocating the bacterial membrane.[27,54,55] Table 2 shows a comparison of present work with the literature.

Because the efficiency of nanostructures is proportional to their size and concentration, their oxidative stress is directly proportional to these factors.[56−58] Bacteria die in response of extrusion and bulging of cytoplasmic contents due to reactive oxygen species (ROS) enclosing their peripheral membranes.[59] When cations engage with negative constituents of microbial cells in a significant amount, the microorganisms collapse.[60,61] When cations impair the bacterial ribosomal function and enzymatic degradation, micropathogens are unable to reproduce and persist.[62] Apart from their tendency to interfere with bacteria and decrease cell membrane permeability, doped nanocomposites have the potential to disrupt critical metabolic activities.[63] Antibiotics may be able to contend infectious diseases by blocking enzymes necessary for bacterial survival, which is the key virulence factor involved in the disease.[64]

3. CONCLUSIONS

rGO−ZnO hybrids were synthesized successfully by the co-precipitation method. XRD results revealed the hexagonal structure of sediments. The peaks shifted toward higher 2θ°, and the intensity of peak (101) decreased gradually with the increasing concentration of rGO. Formation of rods with increasing agglomeration was observed in TEM. Raman spectra showed the characteristic peaks of ZnO at 840 and 1149 cm^{-1}, and the presence of rGO can be confirmed by the D and G bands around 1350 and 1590 cm^{-1}. All samples were positive for the antibacterial action toward bacterial pathogens. The findings indicated an additive impact between the synthesized samples and inhibitory zones. As compared to Gram-positive bacteria, pristine and doped specimen showed remarkable antibacterial activity against Gram-negative bacteria.

4. EXPERIMENTAL SECTION

Zinc nitrate tetrahydrate ($Zn(NO_3)_2{\cdot}4H_2O$, 98%) and sodium hydroxide (NaOH, 98%) were purchased from Sigma-Aldrich (Germany), polyvinylpyrrolidone (PVP, Mw 40,000) from Sigma-Aldrich (USA), acetic acid (CH_3COOH, Mw 60.05) from Panreac Quimica Sau (E.U), and graphene oxide (GO) and used without further purification.

4.1. Synthesis of ZnO Nanostructures. The synthesis of ZnO nanostructures is carried out by the co-precipitation method. $Zn(NO_3){\cdot}4H_2O$ (0.5 M) was prepared in deionized water. Colloidal solution was stirred for 30 min at 80 °C. Subsequently, a desired amount of NaOH was added dropwise to maintain pH ∼ 11, and the formation of precipitates was observed. The stirred solution was centrifuged several times with DI water and ethanol, and the isolated precipitates were dried overnight at 150 °C and ground to a fine powder.

4.2. Synthesis of rGO−ZnO Hybrid Nanostructures. $Zn(NO_3){\cdot}4H_2O$ was stirred with 0.05% PVP in 1% acetic acid for 30 min to form the $Zn(NO_3){\cdot}4H_2O$-PVP complex. Various concentrations of GO (10, 20, 30, and 40 mg) were added to the above mixture and sonicated for 24 h. To keep the pH ∼ 11, NaOH was added dropwise under vigorous stirring at 80 °C. The precipitates were centrifuged twice at 7500 rpm. The obtained product was dried overnight at 150 °C, and a fine powder was obtained by mechanical grinding. The prepared samples were denoted as ZnO and rGO−ZnO (S-1, S-2, S-3, and S-4), with GO concentrations of 10, 20, 30, and 40 mg.

4.3. Bacterial Purification and Identification. Sheep (ovine) milk specimens showing clinical mastitis were procured from farm lands in Punjab (Pakistan) and cultured on 5% sheep blood agar (SBA). To recover *E. coli* and *S. aureus*, the grown isolates were further purified using triplet streaking on MacConkey Agar (MA) and mannitol salt agar (MSA). To assess the morphological and biochemical features of pure isolates, Gram staining, catalase, and coagulase test procedures were actualized.

4.4. Antimicrobial Activity. The antimicrobial effectiveness of the fabricated nanomaterial was tested using a well diffusion assay with isolated *E. coli* and *S. aureus* bacteria swabbed on MA and MSA, separately. Under a sterile environment, wells with 6 mm diameter were shaped on the MA and MSA plates, and various concentrations (500 and 1000 μg/0.05 mL) were poured into each well as a minimum and maximum dosage, correspondingly, in contrast to ciprofloxacin (5 μg/0.05 mL) and DI water (0.05 mL). The antibacterial effectiveness was assessed by calculating the inhibition areas in millimeters (mm) during an overnight incubation at 37 °C with a Vernier caliper.[56]

4.5. Material Characterization. The samples were analyzed using an X-ray diffractometer (model: PAN Analytical Xpert-PRO) with Cu−K radiation (= 1.540) to determine the crystal structure and phases. FTIR (Perkin Elmer spectrometer) in the 4000−400 cm^{-1} range was employed to study the associated functional groups. Raman spectra were measured using a DXR Raman microscope (Thermo Scientific) and a 532 nm laser (6 mV). A field emission scanning electron microscope (JSM-6460LV) and a transmission electron microscope (TEM, JEOL JEM 2100F) were used to examine the morphology. In an air environment, the SDT Q600 (TA Instrument) was used to perform DSC and TGA.

AUTHOR INFORMATION

Corresponding Authors

Muhammad Ikram − *Solar Cell Application Research Lab, Department of Physics, Government College University Lahore, Lahore 54000, Pakistan;* orcid.org/0000-0001-7741-789X; Email: dr.muhammadikram@gcu.edu.pk

https://doi.org/10.1021/acsomega.2c03049
ACS Omega 2022, 7, 26715−26722

Walid Nabgan − *Departament d'Enginyeria Química, Universitat Rovira i Virgili, Tarragona 43007, Spain*; Email: walid.nabgan@urv.cat
Mujtaba Ikram − *Institute of Chemical Engineering and Technology (ICET), University of the Punjab, Lahore 54590, Pakistan*; Email: mujtaba.icet@pu.edu.pk

Authors

Osama Usman − *Department of Physics, University of the Lahore, Lahore 54000, Pakistan*
Namra Abid − *Physics Department, Lahore Garrison University, Lahore 54000 Punjab, Pakistan*
Mohsin Saeed − *Department of Physics, Universiry of the Punjab, Lahore 54000, Pakistan*
Aneeqa Bashir − *Department of Physics, Universiry of the Punjab, Lahore 54000, Pakistan*
Nosheen Mushahid − *Department of Physics, University of the Lahore, Lahore 54000, Pakistan*

Complete contact information is available at: https://pubs.acs.org/10.1021/acsomega.2c03049

Notes

The authors declare no competing financial interest.

■ ACKNOWLEDGMENTS

The authors are gratified to HEC, Pakistan, through project NRPU-20-17615 and University of the Punjab through research grant/Dr. Mujtaba Ikram/No. D/72/Est-l.

■ REFERENCES

(1) Desselberger, U. Emerging and Re-Emerging Infectious Diseases. *J. Infect.* **2000**, *40*, 3−15.
(2) Ohira, T.; Yamamoto, O.; Iida, Y.; Nakagawa, Z. E. Antibacterial Activity of ZnO Powder with Crystallographic Orientation. *J. Mater. Sci. Mater. Med.* **2008**, *19*, 1407−1412.
(3) Jones, N.; Ray, B.; Ranjit, K. T.; Manna, A. C. Antibacterial Activity of ZnO Nanoparticle Suspensions on a Broad Spectrum of Microorganisms. *FEMS Microbiol. Lett.* **2008**, *279*, 71−76.
(4) Sahoo, S. Socio-Ethical Issues and Nanotechnology Development: Perspectives from India. *Conference on Nanotechnology*; IEEE, 2010; pp 1205−1210.
(5) Turner, R. J. Metal-Based Antimicrobial Strategies. *Microb. Biotechnol.* **2017**, *10*, 1062−1065.
(6) Yasuyuki, M.; Kunihiro, K.; Kurissery, S.; Kanavillil, N.; Sato, Y.; Kikuchi, Y. Antibacterial properties of nine pure metals: a laboratory study usingStaphylococcus aureusandEscherichia coli. *Biofouling* **2010**, *26*, 851−858.
(7) Gudkov, S. V.; Burmistrov, D. E.; Serov, D. A.; Rebezov, M. B.; Semenova, A. A.; Lisitsyn, A. B. A Mini Review of Antibacterial Properties of ZnO Nanoparticles. *Front. Phys.* **2021**, *9*, 49.
(8) Husen, A. Gold Nanoparticles from Plant System: Synthesis, Characterization and their Application. *Nanoscience and Plant−Soil Systems*; Springer, 2017; pp 455−479.
(9) Chaudhry, Q.; Scotter, M.; Blackburn, J.; Ross, B.; Boxall, A.; Castle, L.; Aitken, R.; Watkins, R. Applications and implications of nanotechnologies for the food sector. *Food Addit. Contam., Part A: Chem., Anal., Control, Exposure Risk Assess.* **2008**, *25*, 241−258.
(10) Kołodziejczak-Radzimska, A.; Jesionowski, T. Zinc Oxide-from Synthesis to Application: A Review. *Materials* **2014**, *7*, 2833−2881.
(11) Ong, C. B.; Ng, L. Y.; Mohammad, A. W. A Review of ZnO Nanoparticles as Solar Photocatalysts: Synthesis, Mechanisms and Applications. *Renew. Sustain. Energy Rev.* **2018**, *81*, 536−551.
(12) Panchal, P.; Paul, D. R.; Sharma, A.; Hooda, D.; Yadav, R.; Meena, P.; Nehra, S. P. Phytoextract Mediated ZnO/MgO Nanocomposites for Photocatalytic and Antibacterial Activities. *J. Photochem. Photobiol., A* **2019**, *385*, 112049.
(13) Naskar, A.; Lee, S.; Kim, K. S. Antibacterial Potential of Ni-Doped Zinc Oxide Nanostructure: Comparatively More Effective against Gram-Negative Bacteria Including Multi-Drug Resistant Strains. *RSC Adv.* **2020**, *10*, 1232−1242.
(14) Khan, M. M.; Harunsani, M. H.; Tan, A. L.; Hojamberdiev, M.; Azamay, S.; Ahmad, N. Antibacterial Activities of Zinc Oxide and Mn-Doped Zinc Oxide Synthesized Using Melastoma Malabathricum (L.) Leaf Extract. *Bioprocess Biosyst. Eng.* **2020**, *43*, 1499−1508.
(15) Yao, S.; Feng, X.; Lu, J.; Zheng, Y.; Wang, X.; Volinsky, A. A.; Wang, L. N. Antibacterial activity and inflammation inhibition of ZnO nanoparticles embedded TiO2nanotubes. *Nanotechnology* **2018**, *29*, 244003.
(16) Qamar, M. T.; Aslam, M.; Ismail, I. M. I.; Salah, N.; Hameed, A. The assessment of the photocatalytic activity of magnetically retrievable ZnO coated γ-Fe2O3 in sunlight exposure. *Chem. Eng. J.* **2016**, *283*, 656−667.
(17) Rao, C. N. R.; Sood, A. K.; Subrahmanyam, K. S.; Govindaraj, A. Graphene: The New Two-Dimensional Nanomaterial. *Angew. Chem., Int. Ed.* **2009**, *48*, 7752−7777.
(18) Katsnelson, M. I. Graphene: Carbon in Two Dimensions. *Mater. Today* **2007**, *10*, 20−27.
(19) Geim, A. K.; Novoselov, K. S. The Rise of Graphene. *Nanoscience and Technology: A Collection of Reviews from Nature Journals*; Nature, 2009; pp 11−19.
(20) Karthik, R.; Thambidurai, S. Synthesis of Cobalt Doped ZnO/Reduced Graphene Oxide Nanorods as Active Material for Heavy Metal Ions Sensor and Antibacterial Activity. *J. Alloys Compd.* **2017**, *715*, 254−265.
(21) Yousefi, R.; Beheshtian, J.; Seyed-Talebi, S. M.; Azimi, H. R.; Jamali-Sheini, F. Experimental and Theoretical Study of Enhanced Photocatalytic Activity of Mg-Doped ZnO NPs and ZnO/RGO Nanocomposites. *Chem.—Asian J.* **2018**, *13*, 194−203.
(22) Bigdeli Tabar, M.; Elahi, S. M.; Ghoranneviss, M.; Yousefi, R. The Role of the Se-Rich and Se-Poor Conditions in the Photocatalytic Performance of ZnSe/RGO Nanocomposites. *Appl. Surf. Sci.* **2020**, *513*, 145819.
(23) Khorramshahi, V.; Karamdel, J.; Yousefi, R. High Acetic Acid Sensing Performance of Mg-Doped ZnO/RGO Nanocomposites. *Ceram. Int.* **2019**, *45*, 7034−7043.
(24) Baghchesara, M. A.; Azimi, H. R.; Ghorban Shiravizadeh, A.; Asri Mat Teridi, M.; Yousefi, R. Improving the Intrinsic Properties of RGO Sheets by S-Doping and the Effects of RGO Improvements on the Photocatalytic Performance of Cu3Se2/RGO Nanocomposites. *Appl. Surf. Sci.* **2019**, *466*, 401−410.
(25) Yousefi, R.; Cheraghizade, M. Semiconductor/Graphene Nanocomposites: Synthesis, Characterization, and Applications. *Applications of Nanomaterials*; Elsevier, 2018; pp 23−43.
(26) Kichukova, D.; Spassova, I.; Kostadinova, A.; Staneva, A.; Kovacheva, D. Facile Synthesized Cu-RGO and Ag-RGO Nanocomposites with Potential Biomedical Applications. *Nanomaterials* **2022**, *12*, 2096.
(27) Elbasuney, S.; El-Sayyad, G. S.; Tantawy, H.; Hashem, A. H. Promising Antimicrobial and Antibiofilm Activities of Reduced Graphene Oxide-Metal Oxide (RGO-NiO, RGO-AgO, and RGO-ZnO) Nanocomposites. *RSC Adv.* **2021**, *11*, 25961−25975.
(28) Thangaraj, P.; Ramalinga Viswanathan, M.; Balasubramanian, K.; Mansilla, H. D.; Contreras, D.; Sepulveda-Guzman, S.; Gracia-Pinilla, M. A. Ultrasound Assisted Synthesis of Morphology Tunable RGO:ZnO Hybrid Nanostructures and Their Optical and UV-A Light Driven Photocatalysis. *J. Lumin.* **2017**, *186*, 53−61.
(29) Liu, R.; Fu, X. W.; Meng, J.; Bie, Y. Q.; Yu, D. P.; Liao, Z. M. Graphene Plasmon Enhanced Photoluminescence in ZnO Microwires. *Nanoscale* **2013**, *5*, 5294−5298.
(30) Krishna, M. B. M.; Man, M. K. L.; Vinod, S.; Chin, C.; Harada, T.; Taha-Tijerina, J.; Tiwary, C. S.; Nguyen, P.; Chang, P.; Narayanan, T. N.; Rubio, A.; Ajayan, P. M.; Talapatra, S.; Dani, K. M. Engineering Photophenomena in Large, 3D Structures Composed of Self-Assembled van Der Waals Heterostructure Flakes. *Adv. Opt. Mater.* **2015**, *3*, 1551−1556.

(31) Biswas, S.; Tiwary, C. S.; Vinod, S.; Kole, A. K.; Chatterjee, U.; Kumbhakar, P.; Ajayan, P. M. Nonlinear Optical Properties and Temperature Dependent Photoluminescence in HBN-GO Heterostructure 2D Material. *J. Phys. Chem. C* **2017**, *121*, 8060−8069.
(32) Alves, A. P. P.; Koizumi, R.; Samanta, A.; Machado, L. D.; Singh, A. K.; Galvao, D. S.; Silva, G. G.; Tiwary, C. S.; Ajayan, P. M. One-Step Electrodeposited 3D-Ternary Composite of Zirconia Nanoparticles, RGO and Polypyrrole with Enhanced Supercapacitor Performance. *Nano Energy* **2017**, *31*, 225−232.
(33) Sharma, R.; Alam, F.; Sharma, A. K.; Dutta, V.; Dhawan, S. K. ZnO Anchored Graphene Hydrophobic Nanocomposite-Based Bulk Heterojunction Solar Cells Showing Enhanced Short-Circuit Current. *J. Mater. Chem. C* **2014**, *2*, 8142−8151.
(34) Wu, Y.; Yun, J.; Wang, L.; Yang, X. Structure and Optical Properties of Mg-Doped ZnO Nanoparticles by Polyacrylamide Method. *Cryst. Res. Technol.* **2013**, *48*, 145−152.
(35) Zhou, X.; Shi, T.; Zhou, H. Hydrothermal Preparation of ZnO-Reduced Graphene Oxide Hybrid with High Performance in Photocatalytic Degradation. *Appl. Surf. Sci.* **2012**, *258*, 6204−6211.
(36) Liu, X.; Pan, L.; Lv, T.; Lu, T.; Zhu, G.; Sun, Z.; Sun, C. Microwave-Assisted Synthesis of ZnO-Graphene Composite for Photocatalytic Reduction of Cr(Vi). *Catal. Sci. Technol.* **2011**, *1*, 1189−1193.
(37) Boukhoubza, I.; Khenfouch, M.; Achehboune, M.; Mothudi, B. M.; Zorkani, I.; Jorio, A. X-Ray Diffraction Investigations of Nanostructured ZnO Coated with Reduced Graphene Oxide. *J. Phys. Conf.* **2019**, *1292*, 012011.
(38) Saravanan, R.; Santhi, K.; Sivakumar, N.; Narayanan, V.; Stephen, A. Synthesis and Characterization of ZnO and Ni Doped ZnO Nanorods by Thermal Decomposition Method for Spintronics Application. *Mater. Charact.* **2012**, *67*, 10−16.
(39) Ali, M.; Sharif, S.; Anjum, S.; Imran, M.; Ikram, M.; Naz, M.; Ali, S. Preparation of Co and Ni Doped ZnO Nanoparticles Served as Encouraging Nano-Catalytic Application. *Mater. Res. Express* **2019**, *6*, 1250d5.
(40) Song, X.; Liu, Y.; Zheng, Y.; Ding, K.; Nie, S.; Yang, P. Synthesis of Butterfly-like ZnO Nanostructures and Study of Their Self-Reducing Ability toward Au3+ Ions for Enhanced Photocatalytic Efficiency. *Phys. Chem. Chem. Phys.* **2016**, *18*, 4577−4584.
(41) Song, K. Interphase Characterization in Rubber Nanocomposites. *Progress in Rubber Nanocomposites*; Elsevier, 2017; pp 115−152.
(42) Seredych, M.; Rossin, J. A.; Bandosz, T. J. Changes in Graphite Oxide Texture and Chemistry upon Oxidation and Reduction and Their Effect on Adsorption of Ammonia. *Carbon* **2011**, *49*, 4392−4402.
(43) Rong, C.; Ma, G.; Zhang, S.; Song, L.; Chen, Z.; Wang, G.; Ajayan, P. M. Effect of Carbon Nanotubes on the Mechanical Properties and Crystallization Behavior of Poly(Ether Ether Ketone). *Compos. Sci. Technol.* **2010**, *70*, 380−386.
(44) Sun, H. Y.; Lien, S. C.; Qiu, Z. R.; Feng, Z. C. Temperature Dependence of Raman Scattering in 4H-SiC. *Mater. Sci. Forum* **2013**, *740*−*742*, 443−446.
(45) Šćepanović, M.; Grujić-Brojčin, M.; Vojisavljević, K.; Bernik, S.; Srećković, T. Raman Study of Structural Disorder in ZnO Nanopowders. *J. Raman Spectrosc.* **2010**, *41*, 914−921.
(46) Wang, R. P.; Xu, G.; Jin, P. Size Dependence of Electron-Phonon Coupling in ZnO Nanowires. *Phys. Rev. B: Condens. Matter Mater. Phys.* **2004**, *69*, 113303.
(47) Ikram, M.; Aslam, S.; Haider, A.; Naz, S.; Ul-Hamid, A.; Shahzadi, A.; Ikram, M.; Haider, J.; Ahmad, S. O. A.; Butt, A. R. Doping of Mg on ZnO Nanorods Demonstrated Improved Photocatalytic Degradation and Antimicrobial Potential with Molecular Docking Analysis. *Nanoscale Res. Lett.* **2021**, *16*, 1−16.
(48) Ferrari, A. C. Raman Spectroscopy of Graphene and Graphite: Disorder, Electron-Phonon Coupling, Doping and Nonadiabatic Effects. *Solid State Commun.* **2007**, *143*, 47−57.
(49) Shanmugasundaram, A.; Boppella, R.; Jeong, Y. J.; Park, J.; Kim, Y. B.; Choi, B.; Park, S. H.; Jung, S.; Lee, D. W. Facile In-Situ Formation of RGO/ZnO Nanocomposite: Photocatalytic Remediation of Organic Pollutants under Solar Illumination. *Mater. Chem. Phys.* **2018**, *218*, 218−228.
(50) Mokhtar, M. M.; SA Abo El, E.; Hassaan, M.; Morsy, M.; Khalil, M. Thermally Reduced Graphene Oxide: Synthesis, Structural and Electrical Properties. *Int. J. Nanoparticles Nanotechnol.* **2017**, *3*, 1.
(51) Lei, Z.; Lu, L.; Zhao, X. S. The Electrocapacitive Properties of Graphene Oxide Reduced by Urea. *Energy Environ. Sci.* **2012**, *5*, 6391−6399.
(52) Hong, R. Y.; Qian, J. Z.; Cao, J. X. Synthesis and Characterization of PMMA Grafted ZnO Nanoparticles. *Powder Technol.* **2006**, *163*, 160−168.
(53) Rodwihok, C.; Wongratanaphisan, D.; Thi Ngo, Y. L. T.; Khandelwal, M.; Hur, S. H.; Chung, J. S. Effect of GO Additive in ZnO/RGO Nanocomposites with Enhanced Photosensitivity and Photocatalytic Activity. *Nanomaterials* **2019**, *9*, 1441.
(54) Thamer, R.; Alsammak, E. Synergistic Effect of Zinc Oxide Nanoparticles and Vancomycin on Methicillin Resistant Staphylococcus Aureus. *J. Life Bio Sci. Res.* **2021**, *2*, 01−06.
(55) Guo, Z.; Xie, C.; Zhang, P.; Zhang, J.; Wang, G.; He, X.; Ma, Y.; Zhao, B.; Zhang, Z. Toxicity and Transformation of Graphene Oxide and Reduced Graphene Oxide in Bacteria Biofilm. *Sci. Total Environ.* **2017**, *580*, 1300−1308.
(56) Haider, A.; Ijaz, M.; Imran, M.; Naz, M.; Majeed, H.; Khan, J. A.; Ali, M. M.; Ikram, M. Enhanced bactericidal action and dye degradation of spicy roots' extract-incorporated fine-tuned metal oxide nanoparticles. *Appl. Nanosci.* **2020**, *10*, 1095−1104.
(57) Ahmed, B.; Solanki, B.; Zaidi, A.; Khan, M. S.; Musarrat, J. Bacterial Toxicity of Biomimetic Green Zinc Oxide Nanoantibiotic: Insights into ZnONP Uptake and Nanocolloid-Bacteria Interface. *Toxicol. Res.* **2019**, *8*, 246−261.
(58) de la Torre, B. G.; Albericio, F. The Pharmaceutical Industry in 2020. An Analysis of Fda Drug Approvals from the Perspective of Molecules. *Molecules* **2021**, *26*, 627.
(59) Ikram, M.; Tabassum, R.; Qumar, U.; Ali, S.; Ul-Hamid, A.; Haider, A.; Raza, A.; Imran, M.; Ali, S. Promising performance of chemically exfoliated Zr-doped MoS2 nanosheets for catalytic and antibacterial applications. *RSC Adv.* **2020**, *10*, 20559−20571.
(60) Altaf, S.; Haider, A.; Naz, S.; Ul-Hamid, A.; Haider, J.; Imran, M.; Shahzadi, A.; Naz, M.; Ajaz, H.; Ikram, M. Comparative Study of Selenides and Tellurides of Transition Metals (Nb and Ta) with Respect to Its Catalytic, Antimicrobial, and Molecular Docking Performance. *Nanoscale Res. Lett.* **2020**, *15*, 1−16.
(61) Guimarães, A. C.; Meireles, L. M.; Lemos, M. F.; Guimarães, M. C. C.; Endringer, D. C.; Fronza, M.; Scherer, R. Antibacterial Activity of Terpenes and Terpenoids Present in Essential Oils. *Molecules* **2019**, *24*, 2471.
(62) Rajan, P.; Vijaya, J.; Jesudoss, S. K.; Kaviyarasu, K.; Kennedy, L.; Jothiramalingam, R.; Al-Lohedan, H. A.; Vaali-Mohammed, M. A. Green-Fuel-Mediated Synthesis of Self-Assembled NiO Nano-Sticks for Dual Applications-Photocatalytic Activity on Rose Bengal Dye and Antimicrobial Action on Bacterial Strains. *Mater. Res. Express* **2017**, *4*, 085030.
(63) Thill, A.; Zeyons, O.; Spalla, O.; Chauvat, F.; Rose, J.; Auffan, M.; Flank, A. M. Cytotoxicity of CeO2 Nanoparticles for Escherichia Coli. Physico-Chemical Insight of the Cytotoxicity Mechanism. *Environ. Sci. Technol.* **2006**, *40*, 6151−6156.
(64) Konieczna, I.; Zarnowiec, P.; Kwinkowski, M.; Kolesinska, B.; Fraczyk, J.; Kaminski, Z.; Kaca, W. Bacterial Urease and Its Role in Long-Lasting Human Diseases. *Curr. Protein Pept. Sci.* **2012**, *13*, 789−806.
(65) Malik, A. R.; Sharif, S.; Shaheen, F.; Khalid, M.; Iqbal, Y.; Faisal, A.; Aziz, M. H.; Atif, M.; Ahmad, S.; Fakhar-e-Alam, M.; Hossain, N.; Ahmad, H.; Botmart, T. Green Synthesis of RGO-ZnO Mediated Ocimum Basilicum Leaves Extract Nanocomposite for Antioxidant, Antibacterial, Antidiabetic and Photocatalytic Activity. *J. Saudi Chem. Soc.* **2022**, *26*, 101438.
(66) Rajaura, R. S.; Sharma, V.; Ronin, R. S.; Gupta, D. K.; Srivastava, S.; Agrawal, K.; Vijay, Y. K. Synthesis, Characterization and

https://doi.org/10.1021/acsomega.2c03049
ACS Omega 2022, 7, 26715−26722

Enhanced Antimicrobial Activity of Reduced Graphene Oxide-Zinc Oxide Nanocomposite. *Mater. Res. Express* **2017**, *4*, 025401.
(67) Dhandapani, P.; AlSalhi, M. S.; Karthick, R.; Chen, F.; Devanesan, S.; Kim, W.; Rajasekar, A.; Ahmed, M.; Aljaafreh, M. J.; muhammad, A. Biological Mediated Synthesis of RGO-ZnO Composites with Enhanced Photocatalytic and Antibacterial Activity. *J. Hazard. Mater.* **2021**, *409*, 124661.
(68) Rajeswari, R.; Prabu, H. G. Synthesis Characterization, Antimicrobial, Antioxidant, and Cytotoxic Activities of ZnO Nanorods on Reduced Graphene Oxide. *J. Inorg. Organomet. Polym. Mater.* **2018**, *28*, 679−693.

https://doi.org/10.1021/acsomega.2c03049
ACS Omega 2022, 7, 26715−26722